Helical variation of density profiles and fluctuations in the tokamak pedestal with applied 3D fields and implications for confinement

R. S. Wilcox,[1, a)] T. L. Rhodes,[2] M. W. Shafer,[1] L. E. Sugiyama,[3] N. M. Ferraro,[4] B. C. Lyons,[5] G. R. McKee,[6] C. Paz-Soldan,[5] A. Wingen,[1] and L. Zeng[2]

[1)] *Oak Ridge National Laboratory, PO Box 2008, Oak Ridge, Tennessee 37831*

[2)] *University of California Los Angeles, Los Angeles, California 90095*

[3)] *Massachusetts Institute of Technology, Cambridge, Massachusetts 02139*

[4)] *Princeton Plasma Physics Laboratory, Princeton, New Jersey 05764*

[5)] *General Atomics, San Diego, California 92121*

[6)] *University of Wisconsin-Madison, Madison, Wisconsin 53706*

(Dated: 26 January 2018)

Small 3D perturbations to the magnetic field in DIII-D ($\delta B/B \sim 2 \times 10^{-4}$) result in large modulations of density fluctuation amplitudes in the pedestal, which are shown using Doppler backscattering measurements to vary by a factor of 2. Helical perturbations of equilibrium density within flux surfaces have previously been observed in the pedestal of DIII-D plasmas when 3D fields are applied and were correlated with density fluctuation asymmetries in the pedestal. These intra-surface density and pressure variations are shown through two fluid MHD modeling studies using the M3D-C1 code to be due to the misalignment of the density and temperature equilibrium iso-surfaces in the pedestal region. This modeling demonstrates that the phase shift between the two iso-surfaces corresponds to the diamagnetic direction of the two species, with the mass density surfaces shifted in the ion diamagnetic direction relative to the temperature and magnetic flux iso-surfaces. The resulting pedestal density, potential, and turbulence asymmetries within flux surfaces near the separatrix may be at least partially responsible for several poorly understood phenomena that occur with the application of 3D fields in tokamaks, including density pump out and the increase in power required to transition from L- to H-mode.

PACS numbers: 52.25.Fi, 52.30.Cv, 52.35.Ra, 52.55.Fa

I. INTRODUCTION

Non-axisymmetric fields are often applied in tokamaks as a mechanism for plasma control. Most often they are used for edge localized mode (ELM) mitigation or suppression using resonant magnetic perturbations (RMPs),[1,2] but there are also applications for rotation control via neoclassical toroidal viscosity[3,4] and schemes for tearing mode stabilization using 3D fields to align locked modes with electron cyclotron current drive systems.[5]

Several unintended consequences of the application of 3D fields, however, are currently not well understood. The first is a nearly ubiquitous phenomenon known as "density pumpout", where the plasma particle confinement is reduced with the application of 3D fields, particularly in the edge, without a significant modification of the temperature profile.[2,6,7] Another is the increase to the heating power necessary to transition into H-mode as 3D fields are applied.[8] Although this increase in the power threshold is well documented, there is no theoretical understanding of the mechanism for this change. For ITER, this could be a problem if 3D field application is required before the plasma enters H-mode to suppress the first ELM, because there may not be enough heating power to enter H-mode if the power threshold is increased significantly by these 3D fields. One final mystery that will be mentioned here is the observed 3D modification of scrape off layer temperatures, which is not well matched to modeling.[9] The profile and fluctuation asymmetries presented in this paper are explored with an ultimate aim of addressing these poorly understood phenomena, expanding on work presented in an earlier letter[10] with new fluctuation measurements and modeling analysis.

Section II presents the most clear experimental evidence to date of helically varying density fluctuations in the pedestal with applied 3D fields. In Section III, the possible mechanisms through which 3D fields may impact turbulence are discussed, citing some recent work and new analysis. Section IV then discusses the necessity of two-fluid equilibrium modeling to describe 3D equilibria with significant diamagnetic rotation in the pedestal and presents modeling results. In Section V, some possible implications of these pedestal asymmetries for confinement in H-mode tokamaks are mentioned, and Section VI offers a summary and conclusions.

II. ANTI-CORRELATED DENSITY FLUCTUATION RESPONSE TO 3D PHASE FLIPS

Doppler backscattering (DBS) is used in the DIII-D tokamak to measure mid-k density fluctuations,[11] here in the range $k_\theta \approx 3$ cm^{-1}, which corresponds to $\rho_s \sim 0.2 - 0.75$ in the pedestal (ITG/TEM turbulence). For

[a)] wilcoxrs@ornl.gov

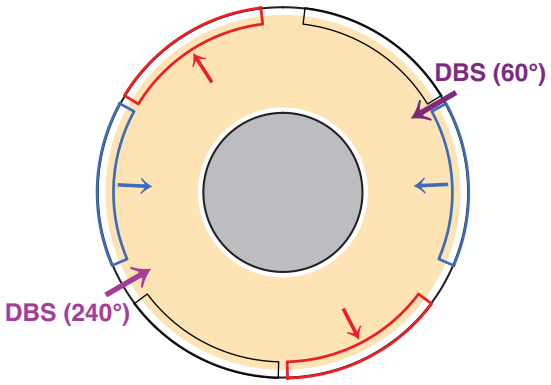

FIG. 1. Top-down view of DIII-D with I-coils and DBS locations indicated. A sample n=2 perturbation for energized I-coils is indicated by red and blue arrows.

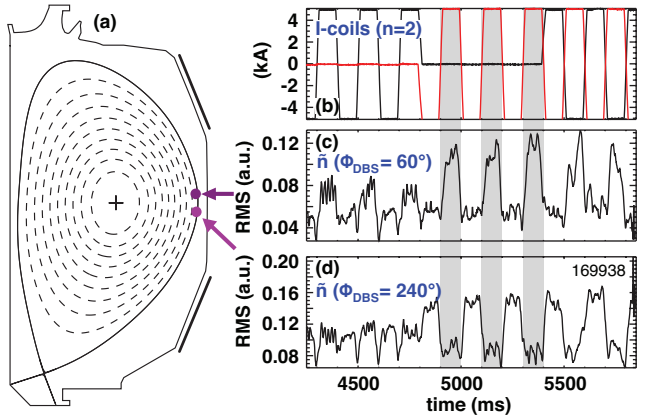

FIG. 2. (a) Plasma cross-section with the DBS measurement locations, time traces from DIII-D discharge 169938 of (b) I-coil current for two sets of upper and lower coils at $\phi = 30°$ (black) and $\phi = 90°$ (red), and DBS fluctuation amplitudes for the systems located toroidally at (c) $\phi = 60°$ and (d) $\phi = 240°$.

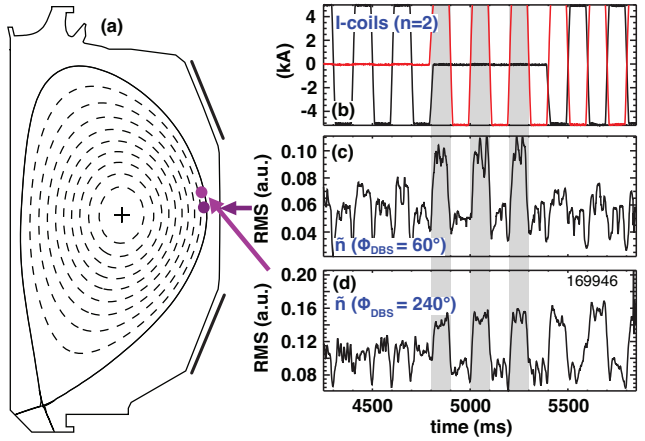

FIG. 3. (a) Plasma cross-section with the DBS measurement locations, time traces from DIII-D discharge 169946 of (b) I-coil current for two sets of upper and lower coils (centered at $\phi = 30°$ in black and $\phi = 90°$ in red), and DBS fluctuation amplitudes for the systems located toroidally at (c) $\phi = 60°$ and (d) $\phi = 240°$.

the experiment presented here, there were two such systems installed in DIII-D, both located on ports at the outboard midplane, but separated toroidally by 180 degrees. Fig. 1 shows a top-down view of the locations of the diagnostic measurements with respect to the I-coils, with the I-coils color coded to demonstrate an example n=2 perturbation. The location of the two rows of coils at a single toroidal location are then given in Fig. 2(a). The upper and lower rows of coils are energized in "even parity" in this case, such that the polarity of two coils at the same toroidal angle is the same. For these experiments, the toroidal field B_T was 2.05 T and the I-coils were energized with approximately 5 kA of current, resulting in a perturbed field of $\delta B/B \sim 2 \times 10^{-4}$.

The fluctuations measured by DBS are mapped to the radial location using the 2D reconstructed equilibrium and the equilibrium density profile, which gives the diagnostic excellent radial resolution in the pedestal region where the density gradient is large. When both DBS systems are tuned to the same wavelength, such that they are observing approximately the same radial location, one might naively expect to measure the same qualitative behavior of the density fluctuations between the two systems on opposite sides of the machine given the small amplitude magnetic perturbations, regardless of the precise poloidal location slightly above or below the midplane. In an axisymmetric system, every "flux tube" is the same, such that the turbulent stability, drive and damping can be calculated for any toroidal location, and the parallel connection along field lines between poloidal locations means that modes extended along a field line would be observed similarly at nearby poloidal locations.

Fig. 2(a) shows the plasma equilibrium cross-section along with the poloidal locations where the two DBS systems measured density fluctuations for DIII-D discharge 169938. Two sample I-coil currents are given in Fig. 2(b), located toroidally at $\phi = 30°$ (black) and $\phi = 90°$ (red). These demonstrate the times at which the field polarity is flipped every 100 ms, as well as the times when the relative phase is rotated every 600 ms (i.e., which coil is not energized during the phase flips, as given by the black coils without arrows in Fig. 1).

The density fluctuation amplitudes measured by DBS and integrated from $1-4$ MHz are presented in Fig. 2(c) for the system located at $\phi = 60°$ and (d) for the system located at $\phi = 240°$. Time slices with the largest change in fluctuation amplitudes between adjacent I-coil phase flips are highlighted in grey. It is clear that the I-coil phase dependence of the fluctuations at the two measurement locations are anti-correlated, such that one amplitude goes up when the I-coil polarity is flipped as the other goes down. These simultaneous measurements demonstrate that the turbulence stability is not consis-

tent on these flux surfaces, where some global n=0 parameter is changing and every flux tube is the same, but rather the turbulence stability is flux tube dependent. Furthermore, the fluctuation amplitudes change by about a factor of 2 between the two I-coil phases, which is a dramatic change in turbulence amplitude for a 3D field perturbation of $\delta B/B \sim 2 \times 10^{-4}$. For locations further inside the plasma, this phase relationship remained the same, but the measured fluctuation amplitude changes were smaller.

Fig. 3 then plots the same data as Fig. 2 for a repeat discharge, 169946, where the DBS system at $\phi = 240°$ is now observing slightly above the midplane as opposed to slightly below, while the system at $\phi = 60°$ is at the same poloidal location as it was in Fig. 3(a). In this case, as seen in the integrated fluctuation amplitudes in Fig. 3(c) and (d), the two diagnostic systems observed a similar relationship between the fluctuation amplitudes and the I-coil phases. The poloidal location change between the measurements in Fig. 2 and Fig. 3 is large enough that the relative behavior of the fluctuation amplitudes at the two locations with respect to I-coil phase was inverted. Given the 180° toroidal separation of the measurement locations, the measurements presented in Fig. 2 and Fig. 3 are consistent with an even toroidal mode structure and poloidal variation with m ≠ 0.

The observed behavior suggests the existence of helical bands of higher and lower density fluctuation amplitudes around the outboard midplane of the plasma. This is consistent with the results from DIII-D which showed that low-k density fluctuation amplitudes at the outboard midplane from the beam emission spectroscopy (BES) diagnostic were tied to the toroidal phase of the applied 3D fields.[10] This relationship was consistent regardless of global confinement and transport changes, with one toroidal phase consistently observing higher fluctuation amplitudes than the other. These new measurements are unique in that they demonstrate both higher and lower fluctuation amplitudes simultaneously at two different locations, demonstrating more definitively that the locally measured turbulence is dependent on the location of the diagnostic relative to the applied fields. ELMs were also present for most of the I-coil phases in the case shown here, demonstrating that this turbulence asymmetry phenomenon is independent of the ELM suppression mechanism, since previous observations were made in ELM-suppressed plasmas.[10]

III. TURBULENCE DRIVE AND DAMPING TERMS MODIFIED BY 3D FIELDS

There are several possible explanations for the observed changes to turbulence amplitudes with the application of 3D fields. A few of these mechanisms are aggregated here as a brief review of the possible modifications to turbulence in the presence of small non-axisymmetric fields.

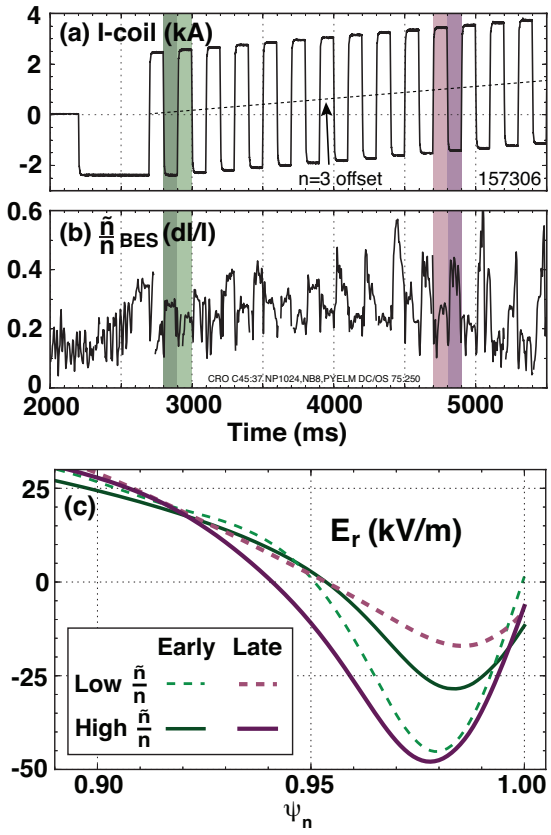

FIG. 4. (a) Sample I-coil current for n=3 toroidal phase flips during an error field offset ramp, (b) integrated fluctuations from BES at $\psi_N = 0.98$ and (c) edge E_r profiles for several time slices, with the colors of the curves corresponding to the times highlighted in (a) and (b).

A. Equilibrium flow shear damping

Modifications to turbulent fluctuations and transport in tokamaks are often attributed to equilibrium E×B rotation shear, due to its dominant and well-documented role in the suppression of turbulence in the H-mode pedestal.[12] Fig. 4, however, presents observations that decouple the edge rotation shear from the observed modulation of pedestal fluctuations as the toroidal phase of the applied 3D fields is changed in DIII-D.

In an ELM-suppressed case that has also been presented previously,[10] an offset ramp was superimposed on top of a series of n=3 I-coil toroidal phase flips. Fig. 4 (a) and (b) give the I-coil current and normalized integrated low-k density fluctuation amplitude (wave number $k < 2 - 3$ cm^{-1}) from the beam emission spectroscopy diagnostic (BES), respectively, for DIII-D discharge 157306. The fluctuations were integrated from $75 - 250$ kHz. A primary conclusion of the previous work was that the relative fluctuation amplitude observed by BES is consistently correlated with the I-coil toroidal phase, as opposed to the global n=0 confinement changes during the n=3 offset ramp. Although the BES data has

more high frequency noise than the DBS data presented in Figures 2 and 3, the trend is clear that the locally observed fluctuations always increase when the I-coil current transitions from positive to negative in the given coil set and decrease when the current transitions from negative to positive.

The radial electric field (E_r) in this case trends roughly with the total n=3 fields (applied fields plus intrinsic error fields), where a larger non-axisymmetric field leads to a smaller pedestal pressure and correspondingly smaller edge E_r well. This is demonstrated in Fig. 4(c) by the edge E_r profiles from four example time slices, two adjacent toroidal phases from one time early and one time late in the n=3 offset ramp. The colors of the E_r profiles in Figure 4(c) correspond to the shaded times in Figures 4(a) and (b).

It can be seen in Fig. 4(c) that the E_r relationship between the two I-coil phases are reversed during the two highlighted times. Early in the offset ramp, from 2800 – 3000 ms, the equilibrium with a deeper E_r well and more E_r shear resulted in lower normalized fluctuation amplitudes $\tilde{n}/n$, as one might expect if equilibrium rotation shearing was the primary difference between the turbulence characteristics during the two phases. Late in the ramp, however, from 4700 – 4900 ms, the opposite relationship is present: the equilibrium with a deeper E_r well and more E_r shear actually results in *increased* normalized fluctuation amplitudes. These trends are indicative of profiles across the entire offset ramp; the locally observed fluctuation amplitudes are always correlated with the toroidal phase of the applied n=3 field and are independent of the changes in the E_r profile. This does not mean that the equilibrium E_r profile does not impact the turbulence, it is well established that it does, but here the dominant changes to the turbulence between adjacent I-coil phases can not be explained by changes to equilibrium rotation shearing.

B. Geometric shaping stability terms

When 3D fields are applied, this contorts the magnetic flux surfaces, changing the stability of modes along these field lines. Two important geometric quantities of interest for turbulence stability that are modified with 3D fields are curvature of the magnetic field lines in the direction normal to the flux surface (the "normal curvature"), which increases the linear growth rate of microturbulence modes roughly linearly with negative values, and local magnetic shear, which acts as a stabilizing term for modes in a manner mathematically similar to the rotation shear.[13,14] It has been found that in particular near rational surfaces, even small resonant magnetic perturbations can lead to significant changes to calculated mode stability due to reductions in the local magnetic shear in the vicinity of the resonant rational surface.[15]

Calculations made for the DIII-D discharge 157306 using the non-linear ideal MHD equilibrium solver VMEC[16] showed that in that case, the perturbed quantities were not modulated significantly in the toroidal direction ($\sim$ 0.1% of the poloidal modulation at the resonant rational surface at the top of the pedestal).[17] Similar calculations for other DIII-D discharges with applied RMPs have produced the same qualitative result.

This is not to say that the local magnetic shear can not have an effect on the turbulence near rational surfaces in DIII-D, only that this is not the case in the equilibria examined so far. Recent experiments and modeling in the ASDEX-Upgrade tokamak have shown a link between observed non-axisymmetric turbulence and a modeled reduction in the local magnetic shear near a resonant rational surface,[18] suggesting that some change to the DIII-D shaping or an increase to the applied field magnitude could produce a similar result. Work is ongoing to compare the ASDEX-Upgrade equilibria with those from DIII-D.

C. Nonlinearly saturated turbulence changes

In principle, zonal flows are known to be modified by deviations from symmetry due to neoclassical trapped particle losses.[19] If the zonal flow response is reduced by applied 3D fields through this mechanism, then it could increase the saturated nonlinear fluctuation amplitudes and their associated turbulence fluxes. Based on nonlinear gyrokinetic simulations using the GTC code, however, it was shown that the nonlinear heat fluxes calculated in the pedestal region ($\psi_n = 0.985$) for a DIII-D equilibrium with applied n=2 fields was not modified significantly relative to the axisymmetric case.[20] Plasma shaping and parameters were similar to the equilibria presented here. The same conclusion was reached even when the applied 3D fields were scaled up by a factor of 10 from the experimentally applied 3D field amplitudes, demonstrating that the surface deformation in this case was well below the threshold for modifying the zonal flow response in a way that was meaningful to the instabilities present.

Some caveats to this GTC modeling should be noted. The underlying equilibrium used by GTC to calculate the fluxes[20] was produced using VMEC, which is an ideal MHD equilibrium solver, so that the terms that are modified here are only the magnetic surface deformation terms as discussed in Section III B. This reinforces the conclusion of the geometric stability term modeling that these surface deformations are not large enough to impact the linear growth rates of the turbulence.[17] But the conclusion that the zonal flow saturation mechanism is not affected may be altered by modifications to the ideal MHD equilibrium, such as non-constant density and potential on the flux surface, which are apparently present in these experimental equilibria.

Another simple consideration is that if zonal flows were the dominant cause of the turbulence changes here, these would have toroidal and poloidal mode numbers of n=0, m=0, which is in contradiction to the DBS measurements

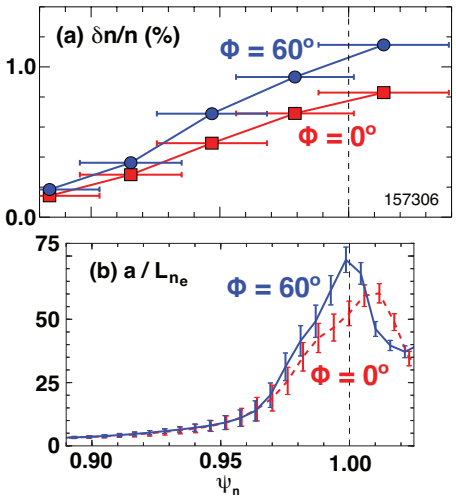

FIG. 5. (a) Integrated low-k density fluctuation amplitudes measured using BES at the outboard midplane for two toroidal phases of applied n=3 perturbations, and (b) the normalized density gradient a/L_{ne} at approximately the same poloidal and toroidal location relative to the n=3 component of the applied field [data from both subplots published previously[10]].

presented here in Fig. 2 for n=2 RMP experiments. So while zonal flows may indeed be impacted by the application of 3D fields (in particular by the two fluid effects that will be discussed in Sec. IV), this is not the cause of the observed modulations to the turbulence.

D. Normalized profile gradients

Turbulent instabilities relevant for magnetic plasma confinement are driven by profile gradients across magnetic surfaces. If these gradients change spatially, then the underlying drive of the instability changes with them, and the turbulent fluctuations may be stronger in some locations than in others. Figure 5 reproduces two measurements that were previously published[10] that suggest that this mechanism is the reason for the toroidal fluctuation asymmetries in the DIII-D discharges examined here with applied 3D fields.

Figure 5(a) shows the measured low-k density fluctuation as measured by the BES diagnostic at the outboard midplane for DIII-D discharge 157306, the n=3 case, around 3750 ms ($\phi = 0°$) and 3850 ms ($\phi = 60°$). The global n=0 profiles for these times were matched, so that the diagnostics were measuring effectively the same plasma equilibria rotated by 60 degrees toroidally. The profile reflectometer in DIII-D measures the density profile at the outboard midplane using fast frequency sweeps. From this, the normalized density gradient $a/L_{n_e} = a\nabla n_e/n_e$ is caculated and plotted in Fig. 5(b). The normalized gradient in the pedestal is larger in the toroidal phase with increased measured density fluctuation amplitudes. The magnitudes of the changes to the normalized gradient and fluctuation amplitudes are also similar between the two toroidal phases, with each diagnostic measuring a $\sim 30-40\%$ increase from the low to the high values of each respective quantity.

While the normalized density gradient a/L_{ne} at the outboard midplane is both measured and modeled to vary with the applied toroidal phase, at the same location, the modeled normalized electron and ion temperature gradients, a/L_{Te} and a/L_{Ti}, do not change as significantly with toroidal phase.[10] This demonstrates that a/L_{ne} is not changing simply because of flux surfaces compressing more in some locations compared to others, which would affect all gradients similarly, but rather the density is redistributing within the flux surfaces in the pedestal.

IV. TWO FLUID MODELING OF PEDESTAL PERTURBATIONS

Standard single fluid MHD models can be a good approximation of equilibria in magnetized plasmas. This is the case even if the plasma is three dimensional, as VMEC demonstrates in stellarators,[16] or if there is rotation in an axisymmetric equilibrium that is large enough in the ordering that it can not be neglected. If both of these modifications are present in the same equilibria, however, then two fluids are required to describe the equilibrium.[21] The 3D pedestal profile effects presented in this paper cannot be explained using single fluid plasma models,[17] but are qualitatively captured by the two fluid modeling first introduced in a previous publication[10] and now expanded here.

The momentum equations for electrons and ions can be expressed as

$$\vec{E} + \vec{v}_e \times \vec{B} + \frac{\nabla p_e}{en} = \eta \vec{J} \tag{1}$$

$$\vec{E} + \vec{v}_i \times \vec{B} - \frac{\nabla p_i}{en} = \frac{\rho}{en}(\vec{v}_i \cdot \nabla)\vec{v}_i, \tag{2}$$

where $\vec{E}$ is the electric field, $\vec{B}$ is the magnetic field, $\vec{v}_e$ and $\vec{v}_i$ are the electron and ion fluid velocities, p_e and p_i are the electron and ion pressure, η is the plasma resistivity, $\vec{J}$ is the current density, e is the elementary charge, n is the plasma density and ρ is the mass density. Quasi-neutrality is assumed in all of the calculations presented here.

If the quantities from Equations 1 and 2 are perturbed and expanded linearly in the toroidal direction such that $A \rightarrow Ae^{iN\phi}$ (where N is the toroidal mode number) and the quadratic terms are discarded, the perturbed toroidal rotation velocity $\tilde{v}_{j\phi}$ for each species j can be expressed

as

$$B^2\tilde{v}_{j\phi} = BB_\phi\tilde{v}_{j\|} + B\tilde{B}v_{\phi 0} + \tilde{E}_r \times B_\theta - E_\theta \times \tilde{B}_r - \frac{1}{q_j n}(B_\theta \times \nabla_r \tilde{p}_j + \tilde{B}_\theta \times \nabla_r p_j) + \frac{\tilde{n}}{n}\frac{B_\theta \times \nabla_r p_j}{q_j n} + \gamma\frac{\rho}{en}[\tilde{B}_\theta \times (v_\phi^2/R) + B \times (v_\phi \cdot iN\tilde{v}_r)], \quad (3)$$

where tildes indicate perturbed quantities, q_j is the charge of species j, R is the major radial location, γ is 1 for ions and 0 for electrons, and the coordinate system here uses minor radial direction r, poloidal angle θ and toroidal angle ϕ. The first line to the right of the equal sign in Eq. 3 are terms that are each the same for electrons and ions. The final line is only included for the ion species, but is small relative to the other terms. One can see then that the fluid velocities differ for electrons and ions primarily due to the pressure gradient driven terms on the second line of Eq. 3. This provides some insight into the observation that the density fluctuations and normalized density gradients were modulated toroidally primarily in the pedestal region, due to the large pressure gradients there.[10]

In order to model these two fluid effects for DIII-D equilibria, the M3D-C1 code[22] is used here to calculate the linearized two fluid plasma response for a single toroidal harmonic of the perturbing fields (n=3 in this case, beginning with the experimental 2D kinetic equilibrium solution from discharge 157306). There are smaller sidebands of other toroidal harmonics when the I-coils are energized, but the n=3 harmonic is the dominant component of the perturbed field, and will be the sole focus for clarity in this demonstration. The realistic poloidal geometries of the plasma and I-coils are included in the simulation.

To highlight the unique physics elucidated by the two fluid modeling, the modeled electron temperature and density iso-surfaces at the outboard midplane are plotted in Fig. 6 in dashed white lines and solid light blue lines, respectively, for discharge 157306 at 3750 ms as a function of major radius R and toroidal angle ϕ. The background colors are the modeled normalized radial density gradient a/L_{ne} resulting from these perturbations. Because parallel thermal conductivity is high, the electron temperature iso-surfaces plotted here are very much aligned with the magnetic flux surfaces. The thicker dashed white line in Fig. 6 around R = 2.265 m denotes the modeled perturbed separatrix.

Far inside of the pedestal, as seen near R = 2.24 m in Fig. 6, the toroidal phase of the perturbed density and temperature iso-surfaces are mostly aligned with each other (although not entirely). There is some small finite phase shift, which will be discussed in the next section, but density is nearly constant within a given magnetic flux surface. In the pedestal region, however, where the pressure gradient is large and the diamagnetic terms in Eq. 3 become larger, the mass density iso-surfaces become decoupled from the magnetic flux surfaces. As seen closer to the separatrix in Fig. 6, the peaks of the density and temperature iso-surfaces are shifted relative to each other: the density iso-surfaces toward the ion diamagnetic direction and the temperature/magnetic flux iso-surfaces toward the electron diamagnetic direction.

One primary result of these phase shifted density and magnetic iso-surfaces is a dramatic variation in the resulting normalized density gradient, plotted with the background colors in Fig. 6. The modulation of the normalized gradients are not aligned with the modulation of the magnetic flux surfaces, so that the local turbulence drive within a flux surface changes depending on the toroidal and poloidal location with respect to the applied 3D fields. This would drive both pressure and density gradient driven turbulence more strongly in the helical flux tubes with increased gradients relative to the flux tubes with decreased normalized gradients, resulting in helical bands of increased fluctuations. These helical bands of increased fluctuation amplitudes are precisely what has been observed, as presented in Sec. II.

The spatial scale in Fig. 6 is extremely out of proportion in order to demonstrate the toroidal variation. The toroidal domain here represents over 14 m in real space, while the radial domain extends less than 3 cm. These plotted perturbations are for a given poloidal location (Z = 0), but the features are extended helically along field lines, such that a given flux bundle would consistently have a larger or smaller normalized gradient along the outboard side of the machine. Parallel pressure gradients are then still relatively small here, as the distances between regions of modeled low and high density along a field line are long, especially compared to the very large cross-field gradients.

One other note here is that the thermal ion banana orbit width and the pedestal width are both about 1 cm at the outboard midplane, so there will certainly be some kinetic effects that are not included in the fluid modeling.

A. Iso-surface phase shift

The dominant physics effect observed here is a phase shift between the iso-thermal and iso-density surfaces that exists in the pedestal when two fluid effects are included in the modeling. To demonstrate this phase shift between the perturbations of the two fluids, the modeled cross phase between the perturbed density and electron temperatures is plotted in Fig. 7(a) for the n=3 case (DIII-D discharge 157306 at 3750 ms). Because the modeling is linearized, this cross phase is independent of the amplitude of the applied fields. It should be emphasized that this is the modeled cross phase between the perturbed *equilibrium* density and temperature, as opposed to the fluctuation density-temperature cross phases that are typically studied with regards to drift wave turbulence and its associated transport.

The absolute value of the radial gradient of the total pressure $|\nabla P|$ is then plotted in Fig. 7(b), as calculated

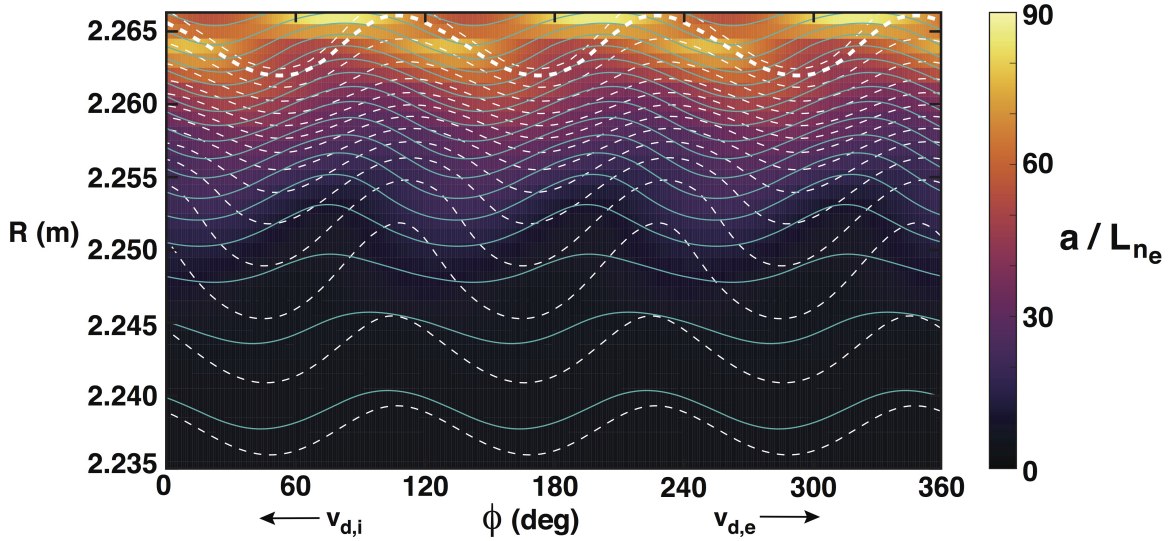

FIG. 6. Modeled density (solid light blue) and T_e (dashed white) iso-surfaces at the outboard midplane, along with the resulting normalized density gradient a/L_{ne} as the background color. T_e iso-surfaces are considered aligned with magnetic flux surfaces.

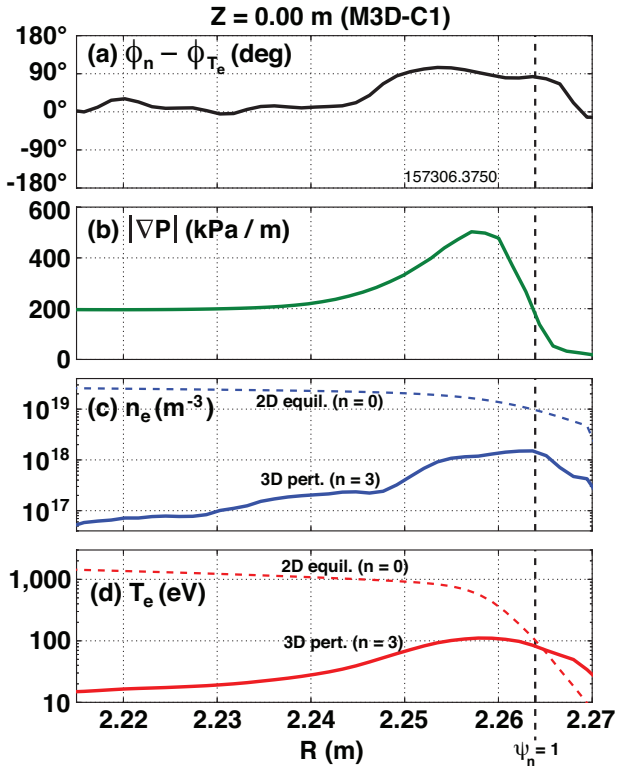

FIG. 7. (a) Modeled toroidal cross phase between equilibrium density and T_e iso-surfaces, (b) the absolute value of the gradient of the total pressure, (c) the n=0 (dashed blue) and perturbed n=3 (solid blue) components of the density, and (d) the n=0 (dashed red) and perturbed n=3 (solid red) components of the electron temperature. All quantities are taken along a horizontal chord the outboard midplane, Z = 0.00 m, and the separatrix is labeled as $\psi_n = 1$.

from the 2D, n=0 component of the equilibrium. This quantity was originally calculated by kinetic equilibrium reconstruction, and was used as an input in the M3D-C1 3D response calculations. It is clear that the radial region where the cross phase deviates from zero (where the n_e and T_e perturbations and iso-surfaces are misaligned) corresponds to the peak in the pressure gradient. In the interior of the plasma, where the pressure gradient is smaller than in the pedestal but still finite, there remains some finite phase shift between the iso-surfaces, but the cross phase is smaller and the perturbation amplitudes are smaller than they are in the edge. This qualitative result is consistent at other poloidal locations at the outboard, low-field side of the plasma. The tendency of the cross-phase to stay near either 0 or 90 degrees may be related to the linearization of the MHD equations, but further work is required to determine the quantitative relationship between the input quantities and the cross phase of n_e and T_e perturbations.

The perturbation amplitudes of the 3D response of equilibrium n_e and T_e quantities are then given in Fig. 7(c) and (d), respectively, with a logarithmic axis. The axisymmetric equilibrium values, which sum with the perturbed quantities to determine the final 3D equilibrium, are given as dashed lines. Experimental values of the I-coil currents were used in these calculations. For linearized calculations, the assumption that the perturbations are much smaller than the equilibrium quantities is made to simplify the equations. It is clear from the large amplitude perturbations outside of the separatrix that this assumption is violated, which may explain the overpredicted modeled plasma response relative to the experimental measurements.[10] Non-linear two fluid equilibrium calculations are significantly more difficult than these linearized calculations, but these would be valuable for comparison when they become available.

The complicated interwoven relationship between the parallel and perpendicular particle flows, viscosity, parallel force balance and the resulting self consistent mass density and temperature iso-surfaces will be left to future work.

V. DISCUSSION OF POSSIBLE IMPLICATIONS

Helical bands of increased normalized gradients and fluctuation amplitudes as reported here could have many implications on plasma confinement. Investigation into these effects is ongoing, and this is by no means an exhaustive list, but what is presented here is an initial estimate of the effects that these phenomena may cause based on a few poorly understood observations of plasmas with applied 3D fields.

The pitch angles of magnetic field lines on the outboard side of the tokamak near the I-coils are nearly constant across the outer plasma radius, even across the separatrix. The result of this is that any applied fields with the two rows of I-coils that are energized in a "resonant" configuration for field lines at the top of the pedestal will result in resonant perturbations all the way out to the scrape-off layer as well. Conversely, non-resonant configurations will result in perturbations from the two I-coil rows that interfere destructively with each other, significantly reducing their perturbations on the plasma at all radial locations. This suggests that any effect caused by the applied 3D fields that is related to these linearized plasma response effects will be minimized with non-resonant applied fields.

A. Increase in power threshold for L-H transition

Previous calculations have shown that the turbulence-driven Reynolds stress at the confined plasma boundary plays a critical role in the development of the edge transport barrier that defines H-mode confinement.[23] If the edge turbulence is significantly modified by the application of small 3D fields so that it is no longer toroidally symmetric, then this would certainly impact the associated Reynolds stress and resulting plasma rotation. This could be the cause of the observed increase in the L-H power threshold with applied 3D fields,[8] but significant modeling and experimental comparisons are required to determine if either turbulence modulation or profile asymmetries are responsible.

The detailed nonlinear interactions between the turbulence, Reynolds stress, and equilibrium flows during the L to H mode transition have only very recently been calculated for an axisymmetric system,[23] so expanding these calculations to include the effects of 3D turbulence may take a significant dedicated effort. It has been shown that the simple 3D topology of the magnetic flux surface do not significantly modify the turbulence in gyrokinetic calculations.[17] This gives hope that some simple modifications to the axisymmetric calculations to include helically varying turbulence would provide useful insight into the impact that these fluctuation modulations have on the confinement transition, without requiring fully 3D simulations.

B. 3D spatial modulation of fluxes into scrape off layer

Many studies have explored both the experimental and modeled modification of the heat flux to divertor material surfaces when 3D fields are applied in tokamaks,[24,25] but agreement between the measured and modeled scrape-off layer temperatures has been difficult to come by given existing plasma response models and simple diffusive transport.[9] The inclusion of toroidally and poloidally varying transport fluxes in the modeling may improve agreement with observed quantities, if asymmetric heat and particle fluxes onto open field lines are a significant contribution to scrape-off layer dynamics. Preliminary modeling shows that, in principle, toroidal modulation of heat diffusivity would produce 3D structures in the heat flux pattern at the divertor, even with axisymmetric fields.[26] This suggests that the modification to heat flux calculated using the full 3D field structure along with realistic spatial variation of diffusivities could be significant. These calculations will be the subject of future work.

C. Density pumpout

While it has been shown that the reduction in core rotation due to the application of 3D fields can lead to a reduction in core particle confinement,[27] the canonical "density pumpout" often tends to have its largest effects on the density profile near the plasma boundary, where the separatrix density and pedestal density gradients are reduced with the application of 3D fields.[2] These edge density changes are poorly understood, although there are models for an increase in fluxes in the pedestal due to magnetic field ripple resulting from partially screened islands.[28] Other models invoke the stochastization of edge flux surfaces,[29] but this parallel transport mechanism would seem to flatten the electron temperature profile as well, contrary to experimental observations.

In modern tokamaks, the thermal sourcing is large relative to the particle sourcing, so that in equilibrium, the corresponding fluxes are similarly disproportionate. For a representative H-mode discharge in DIII-D, the electron thermal diffusivity (χ_e) was calculated to be significantly larger than the particle diffusivity (D) in the pedestal, $\chi_e \approx 0.4$ m^2/s compared to D $\approx 0.02 - 0.05$ m^2/s where these quantities were at their minimum at $\psi_N = 0.97$.[30] If some transport mechanism then additively increased the diffusivity of heat and particles similarly, the result would be a relaxation of the density profile with no comparable modification to the temperature profiles (i.e., density pumpout).

When magnetic flux surfaces in the pedestal have bands of density modulation, this will lead to a Boltzmann potential response and a corresponding poloidal electric field E_θ in the toroidal cross-section between regions of positive and negative perturbations. In the rotating plasma frame, these would act as a fluctuating MHD-like mode, providing some additional particle and thermal fluxes. This could be a plausible explanation for the observed density pumpout, although this is somewhat speculative without further modeling and comparisons to experimental observations.

It has been shown that density pumpout scales roughly with the plasma rotation, and goes to zero when the net injected torque is approximately equal and opposite that of the neoclassical toroidal viscosity.[31] Any viable model of density pumpout would need to sufficiently explain this key observation. The model presented in the previous paragraph would pass this initial test, as the electrostatic fields would drive more transport as the mode frequency in the plasma frame increased.

VI. SUMMARY AND CONCLUSIONS

Non-axisymmetric structures consistent with helical bands of increased density fluctuations have been observed in the pedestal of the DIII-D tokamak during the application of 3D fields. These fluctuation asymmetries have been correlated with an increase in the normalized density gradients at these locations, which has also been measured and has been corroborated with modeling.

A two fluid plasma response model is required to properly resolve these effects in the pedestal. This is due to the large diamagnetic rotation term resulting from the steep pressure gradient in this radial region, which drives ions and electrons in different directions and acts to decouple the electron and ion fluids. When two fluids are included in the model, the density and temperature isosurfaces are shown to be misaligned in the pedestal, resulting in a significant helical modulation to the normalized density gradient. Locations where the normalized density gradient in the pedestal were shown to be modulated toroidally corresponded to a similar increase in the density fluctuations, suggesting that the 3D-modulated equilibrium gradient drives the turbulence.

There are many possible implications of these intra-surface density gradients in the pedestal, which have only been briefly mentioned here. Future work will explore the impacts of the effects illustrated here on density pumpout, 3D heat flux features in the divertor and the increase to the L-H power threshold with the application of 3D fields.

ACKNOWLEDGMENTS

This material is based upon work supported by the U.S. Department of Energy, Office of Science, Office of Fusion Energy Sciences, using the DIII-D National Fusion Facility, a DOE Office of Science user facility, under Awards DE-AC05-00OR22725, DE-FG02-99ER54527, DE-AC02-09CH11466, DE-FG02-08ER54999, DE-FG02-08ER54984 and DE-FC02-04ER54698. DIII-D data shown in this paper can be obtained in digital format by following the links at `https://fusion.gat.com/global/D3D_DMP`.

This report was prepared as an account of work sponsored by an agency of the United States Government. Neither the United States Government nor any agency thereof, nor any of their employees, makes any warranty, express or implied, or assumes any legal liability or responsibility for the accuracy, completeness, or usefulness of any information, apparatus, product, or process disclosed, or represents that its use would not infringe privately owned rights. Reference herein to any specific commercial product, process, or service by trade name, trademark, manufacturer, or otherwise, does not necessarily constitute or imply its endorsement, recommendation, or favoring by the United States Government or any agency thereof. The views and opinions of authors expressed herein do not necessarily state or reflect those of the United States Government or any agency thereof.

[1] T. E. Evans, R. A. Moyer, P. R. Thomas, J. G. Watkins, T. H. Osborne, J. A. Boedo, E. J. Doyle, M. E. Fenstermacher, K. H. Finken, R. J. Groebner, M. Groth, J. H. Harris, R. J. La Haye, C. J. Lasnier, S. Masuzaki, N. Ohyabu, D. G. Pretty, T. L. Rhodes, H. Reimerdes, D. L. Rudakov, M. J. Schaffer, G. Wang, and L. Zeng, "Suppression of Large Edge-Localized Modes in High-Confinement DIII-D Plasmas with a Stochastic Magnetic Boundary," Physical Review Letters **92** (2004).

[2] M. R. Wade, R. Nazikian, J. S. deGrassie, T. E. Evans, N. M. Ferraro, R. A. Moyer, D. M. Orlov, R. J. Buttery, M. E. Fenstermacher, A. M. Garofalo, M. A. Lanctot, G. R. McKee, T. H. Osborne, M. A. Shafer, W. M. Solomon, P. B. Snyder, W. Suttrop, A. Wingen, E. A. Unterberg, and L. Zeng, "Advances in the physics understanding of ELM suppression using resonant magnetic perturbations in DIII-D," Nuclear Fusion **55**, 023002 (2015).

[3] A. J. Cole, J. D. Callen, W. M. Solomon, A. M. Garofalo, C. C. Hegna, M. J. Lanctot, H. Reimerdes, and the DIII-D Team, "Observation of Peak Neoclassical Toroidal Viscous Force in the DIII-D Tokamak," Physical Review Letters **106** (2011).

[4] N. Logan, J.-K. Park, C. Paz-Soldan, M. Lanctot, S. Smith, and K. Burrell, "Dependence of neoclassical toroidal viscosity on the poloidal spectrum of applied nonaxisymmetric fields," Nuclear Fusion **56**, 036008 (2016).

[5] F. Volpe, A. Hyatt, R. La Haye, M. Lanctot, J. Lohr, R. Prater, E. Strait, and A. Welander, "Avoiding Tokamak Disruptions by Applying Static Magnetic Fields That Align Locked Modes with Stabilizing Wave-Driven Currents," Physical Review Letters **115** (2015).

[6] E. Unterberg, O. Schmitz, T. Evans, R. Maingi, N. Brooks, M. Fenstermacher, S. Mordijck, R. Moyer, and D. Orlov, "The effects of an open and closed divertor on particle exhaust during edge-localized mode suppression by resonant magnetic perturbations in DIII-D," Nuclear Fusion **50**, 034011 (2010).

[7] O. Schmitz, T. Evans, M. Fenstermacher, M. Lehnen, H. Stoschus, E. Unterberg, J. Coenen, H. Frerichs, M. Jakubowski, R. Laengner, C. Lasnier, S. Mordijck, R. Moyer, T. Osborne, H. Reimerdes, D. Reiter, U. Samm, B. Unterberg, and the DIII-D and TEXTOR teams, "Resonant features of energy and particle transport during application of resonant

magnetic perturbation fields at TEXTOR and DIII-D," Nuclear Fusion **52**, 043005 (2012).

[8]P. Gohil, T. Evans, M. Fenstermacher, J. Ferron, T. Osborne, J. Park, O. Schmitz, J. Scoville, and E. Unterberg, "L-h transition studies on DIII-D to determine H-mode access for operational scenarios in ITER," Nuclear Fusion **51**, 103020 (2011).

[9]J. Lore, A. Briesemeister, N. Ferraro, H. Frerichs, B. Lyons, A. McLean, J.-K. Park, and M. Shafer, "Pedestal-to-wall 3d fluid transport simulations on DIII-D," Nuclear Fusion **57**, 056025 (2017).

[10]R. Wilcox, M. Shafer, N. Ferraro, G. McKee, L. Zeng, T. Rhodes, J. Canik, C. Paz-Soldan, R. Nazikian, and E. Unterberg, "Evidence of Toroidally Localized Turbulence with Applied 3d Fields in the DIII-D Tokamak," Physical Review Letters **117** (2016).

[11]W. A. Peebles, T. L. Rhodes, J. C. Hillesheim, L. Zeng, and C. Wannberg, "A novel, multichannel, comb-frequency Doppler backscatter system," Review of Scientific Instruments **81**, 10D902 (2010).

[12]K. H. Burrell, "Effects of ExB velocity shear and magnetic shear on turbulence and transport in magnetic confinement devices," Physics of Plasmas **4**, 1499–1518 (1997).

[13]H. E. Mynick, P. Xanthopoulos, and A. H. Boozer, "Geometry dependence of stellarator turbulence," Physics of Plasmas **16**, 110702 (2009).

[14]H. Mynick, P. Xanthopoulos, B. Faber, M. Lucia, M. Rorvig, and J. N. Talmadge, "Turbulent optimization of toroidal configurations," Plasma Physics and Controlled Fusion **56**, 094001 (2014).

[15]T. M. Bird and C. C. Hegna, "A model for microinstability destabilization and enhanced transport in the presence of shielded 3d magnetic perturbations," Nuclear Fusion **53**, 013004 (2013).

[16]S. P. Hirshman, W. I. Van Rij, and P. Merkel, "Three-dimensional free boundary calculations using a spectral green's function method," Computer Physics Communications **43**, 143–155 (1986).

[17]R. Wilcox, A. Wingen, M. Cianciosa, N. Ferraro, S. Hirshman, C. Paz-Soldan, S. K. Seal, M. Shafer, and E. Unterberg, "Modeling of 3d magnetic equilibrium effects on edge turbulence stability during RMP ELM suppression in tokamaks," Nuclear Fusion **57**, 116003 (2017).

[18]M. Willensdorfer, T. Cote, C. Hegna, W. Suttrop, H. Zohm, M. Dunne, E. Strumberger, G. Birkenmeier, S. Denk, F. Mink, B. Vanovac, L. Luhmann, and the ASDEX Upgrade Team, "Field-Line Localized Destabilization of Ballooning Modes in Three-Dimensional Tokamaks," Physical Review Letters **119** (2017), 10.1103/PhysRevLett.119.085002.

[19]H. Sugama and T.-H. Watanabe, "Collisionless damping of zonal flows in helical systems," Physics of Plasmas **13**, 012501 (2006).

[20]I. Holod, Z. Lin, S. Taimourzadeh, R. Nazikian, D. Spong, and A. Wingen, "Effect of resonant magnetic perturbations on microturbulence in DIII-D pedestal," Nuclear Fusion **57**, 016005 (2017).

[21]L. E. Sugiyama, To be submitted (2018).

[22]N. M. Ferraro, "Calculations of two-fluid linear response to non-axisymmetric fields in tokamaks," Physics of Plasmas **19**, 056105 (2012).

[23]C. Chang, S. Ku, G. Tynan, R. Hager, R. Churchill, I. Cziegler, M. Greenwald, A. Hubbard, and J. Hughes, "Fast Low-to-High Confinement Mode Bifurcation Dynamics in a Tokamak Edge Plasma Gyrokinetic Simulation," Physical Review Letters **118** (2017), 10.1103/PhysRevLett.118.175001.

[24]A. Briesemeister, J.-W. Ahn, J. Canik, M. Fenstermacher, H. Frerichs, C. J. Lasnier, J. Lore, A. Leonard, M. Makowski, A. McLean, W. Meyer, O. Schmitz, M. Shafer, E. Unterberg, H. Wang, and J. G. Watkins, "Changes in divertor conditions in response to changing core density with RMPs," Nuclear Fusion **57**, 076038 (2017).

[25]H. Frerichs, O. Schmitz, T. Evans, Y. Feng, and D. Reiter, "The pattern of parallel edge plasma flows due to pressure gradients, recycling, and resonant magnetic perturbations in DIII-D," Physics of Plasmas **22**, 072508 (2015).

[26]M. W. Shafer, J. M. Canik, A. R. Briesemeister, J. D. Lore, R. S. Wilcox, A. Wingen, N. M. Ferraro, and G. R. McKee, "Nonaxisymmetric Divertor Striations via 3D Modulations in Upstream Transport," in *APS-DPP Meeting Abstracts* (2016).

[27]S. Mordijck, E. J. Doyle, G. R. McKee, R. A. Moyer, T. L. Rhodes, L. Zeng, N. Commaux, M. E. Fenstermacher, K. W. Gentle, H. Reimerdes, O. Schmitz, W. M. Solomon, G. M. Staebler, and G. Wang, "Changes in particle transport as a result of resonant magnetic perturbations in DIII-D," Physics of Plasmas **19**, 056503 (2012).

[28]J. D. Callen, C. C. Hegna, and A. J. Cole, "Magnetic-flutter-induced pedestal plasma transport," Nuclear Fusion **53**, 113015 (2013).

[29]O. Schmitz, M. Becoulet, P. Cahyna, T. Evans, Y. Feng, H. Frerichs, A. Loarte, R. Pitts, D. Reiser, M. Fenstermacher, D. Harting, A. Kirschner, A. Kukushkin, T. Lunt, G. Saibene, D. Reiter, U. Samm, and S. Wiesen, "Three-dimensional modeling of plasma edge transport and divertor fluxes during application of resonant magnetic perturbations on ITER," Nuclear Fusion **56**, 066008 (2016).

[30]J. Callen, R. Groebner, T. Osborne, J. Canik, L. Owen., A. Pankin, T. Rafiq, T. Rognlien, and W. Stacey, "Analysis of pedestal plasma transport," Nuclear Fusion **50**, 064004 (2010).

[31]C. Paz-Soldan, N. C. Logan, M. J. Lanctot, J. M. Hanson, J. D. King, R. J. L. Haye, R. Nazikian, J.-K. Park, and E. J. Strait, "Decoupled recovery of energy and momentum with correction of n = 2 error fields," Nuclear Fusion **55**, 083012 (2015).